The EMBO Journal (2005) 24, 875–884 | © 2005 European Molecular Biology Organization | All Rights Reserved 0261-4189/05
www.embojournal.org

THE EMBO JOURNAL

Structure of palmitoylated BET3: insights into TRAPP complex assembly and membrane localization

Andrew P Turnbull[1,2], Daniel Kümmel[1], Bianka Prinz[3,4], Caterina Holz[3,4], Jeffrey Schultchen[3,4], Christine Lang[3,4], Frank H Niesen[4,5], Klaus-Peter Hofmann[5], Heinrich Delbrück[4,6], Joachim Behlke[1], Eva-Christina Müller[1], Ernst Jarosch[1], Thomas Sommer[1] and Udo Heinemann[1,6,*]

[1]Max-Delbrück-Centrum für Molekulare Medizin, Berlin, Germany, [2]Protein Structure Factory, c/o BESSY GmbH, Berlin, Germany, [3]Institut für Biotechnologie, FG Mikrobiologie und Genetik, Technische Universität Berlin, Berlin, Germany, [4]Protein Structure Factory, Heubnerweg, Berlin, Germany, [5]Institut für Medizinische Physik und Biophysik, Charité Universitätsmedizin Berlin, Berlin, Germany and [6]Institut für Chemie/Kristallographie, Freie Universität Berlin, Berlin, Germany

BET3 is a component of TRAPP, a complex involved in the tethering of transport vesicles to the *cis*-Golgi membrane. The crystal structure of human BET3 has been determined to 1.55-Å resolution. BET3 adopts an α/β-plait fold and forms dimers in the crystal and in solution, which predetermines the architecture of TRAPP where subunits are present in equimolar stoichiometry. A hydrophobic pocket within BET3 buries a palmitate bound through a thioester linkage to cysteine 68. BET3 and yeast Bet3p are palmitoylated in recombinant yeast cells, the mutant proteins BET3 C68S and Bet3p C80S remain unmodified. Both BET3 and BET3 C68S are found in membrane and cytosolic fractions of these cells; in membrane extractions, they behave like tightly membrane-associated proteins. In a deletion strain, both Bet3p and Bet3p C80S rescue cell viability. Thus, palmitoylation is neither required for viability nor sufficient for membrane association of BET3, which may depend on protein–protein contacts within TRAPP or additional, yet unidentified modifications of BET3. A conformational change may facilitate palmitoyl extrusion from BET3 and allow the fatty acid chain to engage in intermolecular hydrophobic interactions.

The EMBO Journal (2005) **24,** 875–884. doi:10.1038/sj.emboj.7600565; Published online 3 February 2005
Subject Categories: structural biology; membranes & transport
Keywords: α/β-plait; BET3 protein; protein palmitoylation; TRAPP complex; vesicle tethering

*Corresponding author. Max-Delbrück-Centrum für Molekulare Medizin, Forschungsgruppe Kristallographie, Robert-Rössle-Straße 10, 13092 Berlin, Germany. Tel.: +49 30 9406 3420; Fax: +49 30 9406 2548; E-mail: heinemann@mdc-berlin.de

Received: 24 August 2004; accepted: 4 January 2005; published online: 3 February 2005

Introduction

Intracellular targeting and transport of proteins in eukaryotic cells depend on a variety of proteins and protein complexes involved in the coating, budding, release, uncoating, tethering and fusion of vesicles. Vesicle budding commonly relies on formation of a protein coat around the bud and is initiated by the binding of a GTPase on the exit membrane. Subsequently, the GTPase interacts with a GTPase-activating protein, leading to GTP hydrolysis and the recruitment of coat-forming proteins to the vesicle bud. These coat-forming proteins interact with proteins on the membrane, initially leading to polymerization and stabilization of the bud and subsequently to dissection of the vesicle from the membrane (Barlowe, 1995; Springer *et al*, 1999). Vesicle fusion to the target compartments is triggered by membrane proteins termed soluble *N*-ethyl-sensitive factor (NSF) attachment protein (SNAP) receptors or SNAREs that have to be located on both the vesicle (as v-SNARE) and the target membranes (as t-SNARE) and which interact with a number of soluble factors. In addition to the interaction with SNAPs, binding of an AAA ATPase, NSF and membrane-specific multi-protein complexes to the vesicle is essential for tethering and fusion (reviewed by Hay and Scheller, 1997; Nichols and Pelham, 1998; Jahn *et al*, 2003; Bonifacino and Glick, 2004).

The attachment of vesicles to their target membrane is mediated by a Rab GTPase and tethering factors. These tethers are multi-component complexes which are transport process-specific (Lowe, 2000; Whyte and Munro, 2002). For example, a complex called exocyst is involved in the tethering of exocytotic vesicles to the plasma membrane (TerBush and Novick, 1995). Along with the conserved oligomeric Golgi (COG) and Golgi-associated retrograde protein (GARP) complexes, the exocyst has been classified as a quadrefoil tethering complex (Whyte and Munro, 2002). The TRAPP complexes, involved in vesicle transport to the Golgi, are unrelated to the quadrefoil complexes. TRAPP has been reported to act as a guanine nucleotide exchange factor for the Rab GTPase Ypt1p (Jones *et al*, 2000; Wang *et al*, 2000).

The TRAPP I complex, necessary for tethering ER-derived vesicles to the Golgi, comprises approximately equimolar amounts of seven proteins (Bet3p, Bet5p, Trs20p, Trs23p, Trs31p, Trs33p and Trs85p; yeast nomenclature) whose sequences are highly conserved from yeast to plants and mammals (Sacher *et al*, 2000, 2001; Sacher and Ferro-Novick, 2001). The TRAPP II complex that guides vesicles inside the Golgi comprises TRAPP I and three additional proteins: Trs65p, Trs120p and Trs130p. The individual deletion of many TRAPP complex components is lethal (Sacher *et al*, 2000), highlighting their importance for vesicle transport and, possibly, other cellular processes. A tagged human BET3 has been used to purify a human TRAPP complex and to identify its subunits (Gavin *et al*, 2002).

BET3 was identified by a synthetic lethal screen as a yeast gene with a role in targeting and fusion of ER-derived vesicles to the Golgi membrane (Rossi *et al*, 1995). The *bet3-1* mutant showed a defect in secreting invertase, α-factor and carboxypeptidase Y, leading to accumulation of these proteins at the ER-to-Golgi stage of transport prior to SNARE complex formation. Sequence analysis identified two novel motifs, $_{[44]}LX_2\#GX_2\#GX_2LXE_{[57]}$ and $_{[133]}G\#_2XGXL_{[139]}$ (where X represents any amino acid and # corresponds to a hydrophobic residue; human BET3 numbering), conserved between Bet3p and two other TRAPP subunits: Trs31p and Trs33p (Sacher *et al*, 2000). The *bet3-1* mutant, in which the TRAPP complex fails to form, involves alteration of the second conserved glycine residue (G52) in the first motif, underscoring the importance of this motif in Bet3p function (Figure 1).

BET3 is a central subunit of TRAPP that has been used to precipitate the intact tethering complex both from yeast and from human cells (Sacher *et al*, 1998; Gavin *et al*, 2002). As the first step towards a structural characterization of TRAPP, here we present the crystal structure of human BET3, a 20-kDa protein comprising 180 amino acids with 54% identity to its yeast ortholog (Sacher *et al*, 1998). We show BET3 to be dimeric in the crystal and in solution and identify a covalent modification with a palmitate deeply buried within a hydrophobic channel of the protein. These findings have important implications for the architecture of the TRAPP I complex and its mode of Golgi membrane attachment.

Results and discussion

Structure analysis and quality of the model

For affinity purification of BET3, the protein was labeled with a His_6 and a StrepII tag, fused to its N- and C-termini, respectively (corresponding to a construct comprising 200 amino acids). The fusion protein had a calculated molecular mass (M_r) of 22 582 kDa, but eluted from the size-exclusion chromatography column at an M_r of approximately 42 kDa (data not shown).

The structure of BET3 was determined by the single-wavelength anomalous diffraction (SAD) technique and refined using data to 1.55-Å resolution. In general, the quality of the electron density map is good for 151 of the expected 200 residues in the fusion protein, the exception being the loop which connects residues 114 and 121 for which the electron density is weak and segmental flexibility must therefore be assumed. Additionally, the N-terminal 21 and the C-terminal 20 residues, including the affinity tags, are not visible in the electron density map and the structure described here is 12 and nine residues, respectively, shorter than the wild-type protein. The side chains of eight residues (K13, E35, E57, K84, F115, L118, N121 and R170) have weak density associated with them and a further seven side chains (K32, K46, R62, R67, N109, E117 and D120) are disordered and have been truncated to the last visible side chain atom in the final model. In the Ramachandran diagram, all residues of the model are located in the most favorable or additionally allowed regions (89.5 and 10.5%, respectively).

BET3 structure

The BET3 monomer has overall dimensions of approximately $36 \times 42 \times 46$ Å and is constructed from four β-strands and five α-helices which harbor 16 and 39%, respectively, of the residues of the total wild-type polypeptide chain (Figure 2A). In addition, there are two segments of 3_{10}-helix (residues 120–122 and 154–156). The relationship between the elements of secondary structure and their positions in the sequence is presented in the alignment of representative BET3 homologs in Figure 1.

The secondary structural elements of BET3 are arranged in an α/β-plait topology constructed by a twisted, antiparallel,

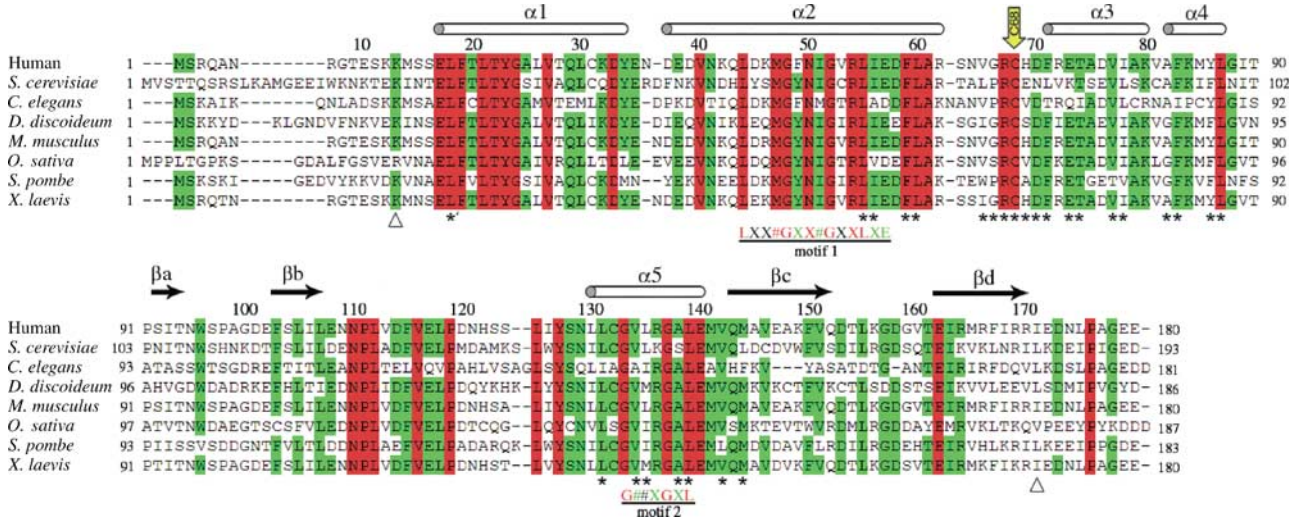

Figure 1 Structure-based multiple sequence alignment of BET3 homologs (Gönczy *et al*, 2000; Glöckner *et al*, 2002; Klein *et al*, 2002; Mammalian Gene Collection (MGC) Program Team, 2002; Wood *et al*, 2002). The secondary structure assignment for human BET3 is represented by cylinders (α-helix) and arrows (β-strand) above the aligned sequences. The triangles below the sequence alignment denote the extent of the assigned human BET3 structure described in this paper (residues 13–171 with respect to the wild-type protein sequence). Fully conserved residues are highlighted in red and additional, highly conserved residues (identical in at least six out of eight aligned sequences) are shaded green. Residues marked by an asterisk below the aligned sequences denote the 27 residues lining the hydrophobic pocket with any atom within 6 Å of the palmitoyl group (including L18 from the adjacent molecule in the BET3 dimer). A yellow arrow points towards the residue C68. The multiple sequence alignment was prepared using *CLUSTAL* (Higgins *et al*, 1992).

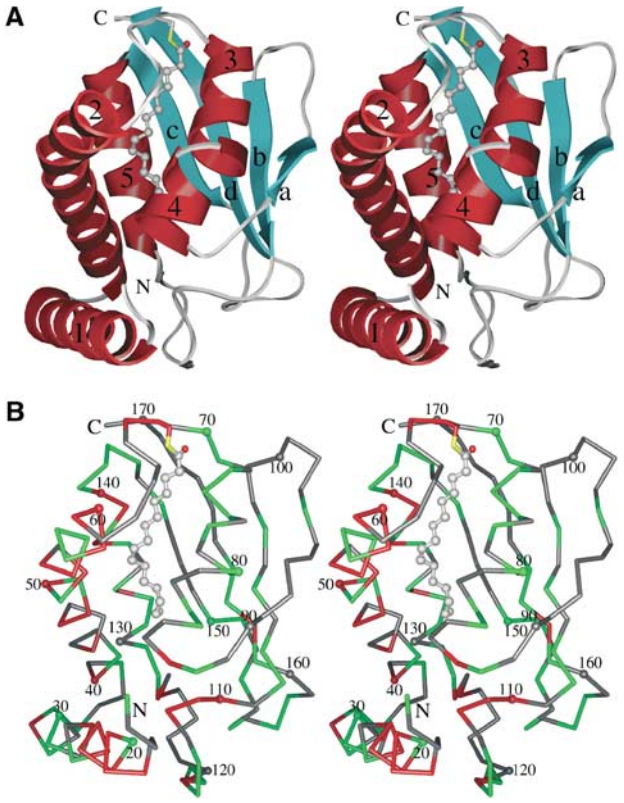

Figure 2 Stereo diagrams of human BET3. (**A**) Schematic representation of the BET3 monomer with the helices and strands colored red and cyan, respectively, and labeled. The palmitate molecule covalently linked to residue C68 through a thioester bond is shown in atom colors (carbon, grey; oxygen, red; sulfur, yellow). (**B**) Cα trace with every tenth residue dotted and numbered. The pattern of sequence conservation across members of the BET3 family is also illustrated using the coloring scheme outlined in Figure 1. Unless otherwise stated, molecular drawings were prepared using CHIMERA (Huang *et al*, 1996).

four-stranded β-sheet on one side, with the helices forming the other side of the structural motif. The pattern of sequence conservation between BET3 homologs indicates that both identical and highly conserved residues are primarily associated with the α-helical face of the molecule (Figure 2B), implying that the β-sheet simply acts as a structural scaffold. Additionally, residues 110–119 in the flexible loop connecting βb to α5 are highly conserved, which suggests that they most likely represent a binding motif for one of the other components of the TRAPP complex. Database searches using VAST (Madej *et al*, 1995; Gibrat *et al*, 1996) and DALI (Holm and Sander, 1993) reveal only limited topological similarities between BET3 and other proteins in the Protein Data Bank (PDB). Specifically, these relate to overlaps of elements of the α/β-plait fold with members of the (α + β) class of proteins. Overall, these similarities do not suggest that the PDB contains any protein with a fold significantly similar to BET3. The recently released structures of mouse BET3 (PDB entries 1VPG, 1WC8, 1WC9) show this protein to share a closely similar fold with human BET3.

BET3 dimer

BET3 forms a dimer around the crystallographic two-fold axis, primarily involving interactions between α1 and, to a lesser extent, α2, α4 and the N-terminal segment of α5 (Figure 3A). Analysis of the molecular surface buried between these subunits shows that the overall accessible surface area (Lee and Richards, 1971) of the BET3 monomer is approximately 9000 Å^2 and that 18% (~1500 Å^2) of the subunit surface area is buried in the crystallographic dimer. Furthermore, the residues located at the dimer interface are highly conserved among the sequences of BET3 homologs (see Figures 1 and 2B). A dimeric arrangement is consistent with the biophysical data reported in this paper and with previous studies, which suggested that there are at least two copies of Bet3p and the other protein subunits in the fully assembled TRAPP complex (Sacher *et al*, 2000).

The dimeric structure of BET3 adopted in the crystal has been additionally confirmed by analytical ultracentrifugation (Figure 3B). The molecular mass (M_r) obtained from sedimentation equilibrium experiments ranged between 43.2 kDa at a protein concentration of 0.62 g l^{-1} and 41.2 kDa at 0.17 g l^{-1}. These values are somewhat lower than the expected value for the dimeric protein, and the positive concentration dependence of M_r is typical for an equilibrium between monomers and dimers. Based on the partial concentrations of both species at all M_r values, an equilibrium dissociation constant (K_d) of 448 ± 34 nM was calculated. Given this affinity, we cannot be certain that in cells BET3 is always present as a dimer, but a dimeric structure seems very likely in compartments enriched in BET3.

BET3 palmitoylation

A striking feature of the BET3 structure is the presence of a hydrophobic pocket within the core of the α-helical face that is approximately 20 Å in length and is formed by the C-terminal end of α2, the loop connecting α2 to α3 and helices α3 to α5 (see Figure 2A). Additionally, within the dimer, the N-terminal end of α1 blocks the base of the pocket adjacent to the subunit interface in the symmetry-related molecule (see Figure 3A). An elongated electron density feature spans the pocket (Figure 4A) in the structures of both the wild-type and the selenomethionine-incorporated protein (data not shown), and is therefore unlikely to be an artifact of crystallization. The shape of the electron density is consistent with it being a palmitate molecule covalently attached to the protein through a thioester linkage to the fully conserved residue C68 (C-S separation 1.9 Å), corresponding to C80 in Bet3p. There are 27 highly conserved and predominantly hydrophobic residues that line the pocket with any atom within 6 Å of the S-palmitoyl group (Figure 4B). In all, 20 are identical in at least six of the eight aligned BET3 sequences, whereas conservative substitutions are seen at the remaining seven positions: V65 (L/I/W), G66 (P/S), H69 (E/N/S/A), I78 (L/V), A82 (G), Y86 (F), and L135 (I/M) (see Figure 1, human BET3 sequence numbering). The recently published structure of mouse BET3 (Kim *et al*, 2005) also shows a fatty acid moiety occupying this site. Palmitate is the most commonly found S-linked fatty acid (Dunphy and Linder, 1998), implying that palmitoylation of BET3 is a natural modification likely to play a functional role. The occlusion of the fatty acid chain inside a hydrophobic crevice of the protein explains why BET3 could be purified as a soluble protein from recombinant yeast cells.

The palmitoylation of BET3 *in vivo* was shown with metabolic labeling of yeast cells expressing BET3, Bet3p and the corresponding cysteine-to-serine mutants (BET3 C68S, Bet3p C80S). Wild-type BET3 and Bet3p purified

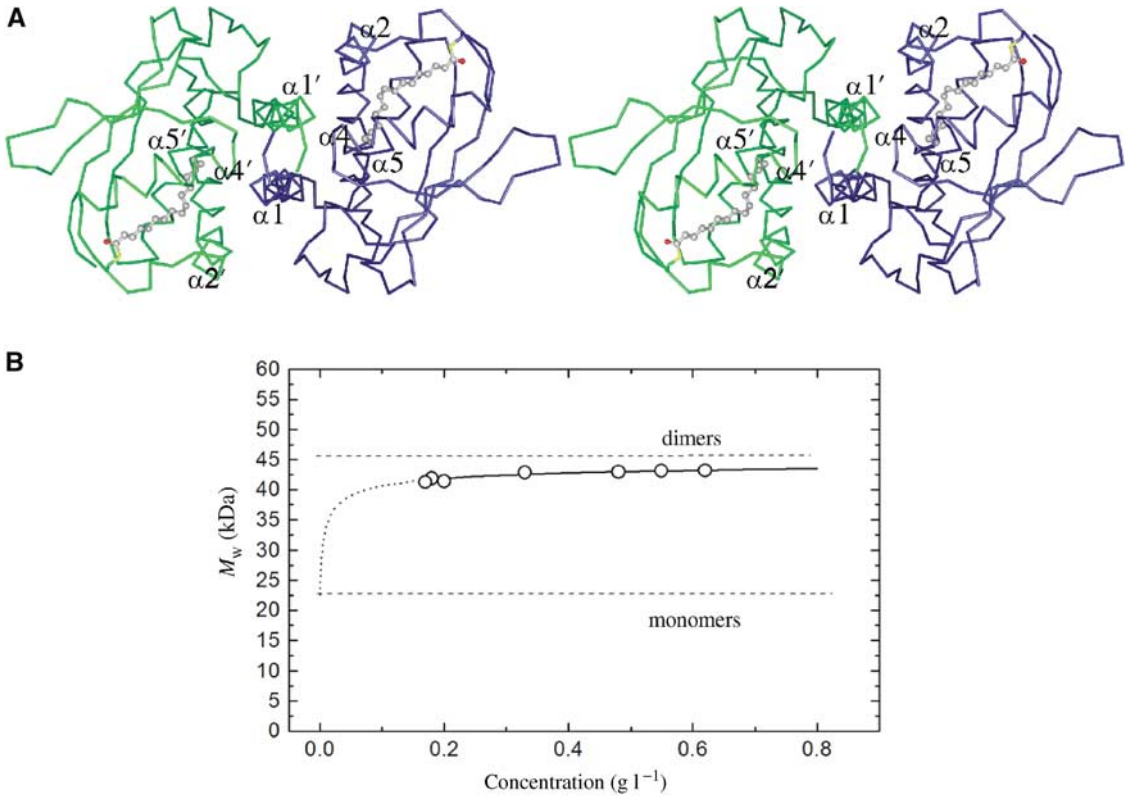

Figure 3 BET3 dimer in the crystal and in solution. (**A**) Cα trace of the BET3 dimer viewed down the crystallographic two-fold axis. Secondary structural elements interacting at the dimer interface are labeled. The two subunits are shown in different colors. (**B**) Concentration dependence of the relative molecular mass (M_r) of BET3 in aqueous buffer from analytical ultracentrifugation, confirming a dimeric quaternary structure. The dotted line represents a monomer–dimer equilibrium fit with a K_d of 448 nM.

from these cultures were palmitoylated as shown by fluorography, whereas no palmitic acid was attached to the mutant proteins (Figure 4C). Differences in intensity are due to the higher expression level of BET3 compared to Bet3p.

The crystal structure of one of the other constituents of the TRAPP complex, the monomeric murine SEDL, an ortholog of yeast Trs20p, has previously been reported (Jang *et al*, 2002). SEDL shares a folding topology identical to the N-terminal regulatory domain of two SNAREs, yeast Ykt6p and mouse Sec22b, despite undetectable sequence homology between these proteins. This has led to the suggestion that SEDL serves regulatory and/or adaptor functions through multiple protein–protein interactions. All three proteins are involved in ER-to-Golgi vesicle transport, and the structural similarities suggest that they may interact with different partners that belong to the same family of proteins. Interestingly, the N-terminal domain of Ykt6p has been implicated in the palmitoylation of the fusion factor Vac8 (Dietrich *et al*, 2004). Ykt6p presents palmitoyl-CoA via its N-terminal domain to Vac8, while transfer to Vac8's SH4 domain occurs spontaneously. Furthermore, Trs20p, the SEDL ortholog in yeast, has been reported to interact with Bet3p on the basis of a genome-wide yeast two-hybrid analysis (Ito *et al*, 2000). This leads to the intriguing possibility that Trs20p (SEDL) exhibits the acyltransferase activity for Bet3p (BET3) palmitoylation.

Possible function of BET3 palmitoylation

Palmitoylation most commonly contributes to the membrane localization of proteins that would otherwise be cytoplasmic, but has also been shown to modulate protein–protein interactions (Dunphy and Linder, 1998). In theory, a single palmitoyl group should be sufficient for membrane association (Peitzsch and McLaughlin, 1993). Since previous studies have shown that TRAPP resides within a Triton X-100-resistant fraction of the Golgi (Sacher *et al*, 2000), we addressed the question whether BET3 palmitoylation is involved in its membrane anchoring. Preparations of cytosolic and membrane fractions from yeast cells expressing BET3 and BET3 C68S, respectively, were analyzed by immunoblotting. Wild-type and mutant BET3 were detectable both in the cytosol and the membrane (Figure 5A). By loading crude cell lysates on a sucrose cushion, it was demonstrated that BET3 as well as BET3 C68S actually are membrane associated and do not form aggregates (not shown). The membrane-bound forms of the proteins cannot be released by extraction with high salt, urea, carbonate and Triton X-100, a feature associated with tightly membrane-associated proteins (Figure 5B). These data show that BET3 is tightly bound to membranes, but that this interaction is only in part mediated through palmitoylation. We take this to suggest that the tight binding to an anchor protein or another modification is additionally required and sufficient to mediate the membrane association of BET3. Since BET3 from the soluble cytosolic pool was purified for crystallization, we cannot exclude the possibility that an additional modification is present in membrane-bound BET3.

To address the question if palmitoylation of BET3 is essential for protein function *in vivo*, BET3 constructs were transformed in a yeast *bet3* deletion strain, and sporulation of

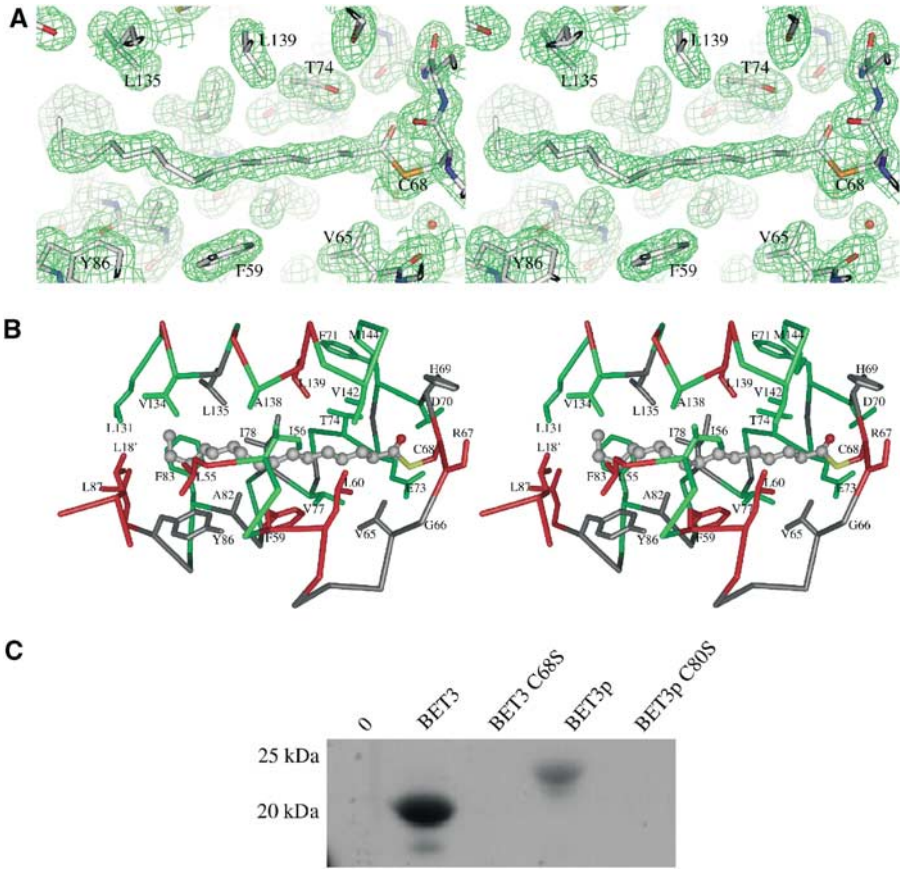

Figure 4 Covalent modification of BET3 with palmitate. (**A**) A portion of the $(2m|F_{obs}|-D|F_{calc}|)\alpha_{calc}$ electron density map centered on the palmitoyl chain and contoured at 1.2σ (prepared using PyMOL; DeLano, 2003). The separation between the C^1-atom position of the palmitoyl group and the side chain S^{γ} of C68 is approximately 1.9 Å, clearly indicating that a thioester bond has formed between these two entities. (**B**) The side chains of the 27 residues lining the hydrophobic pocket with at least one atom residing within 6 Å of the palmitate molecule are shown using the same coloring scheme as outlined in Figure 1. In all, 20 of these residues are identical in at least six of the eight aligned BET3 sequences, whereas conservative substitutions are seen at the remaining seven positions: V65 (L/I/W), G66 (P/S), H69 (E/N/S/A), I78 (L/V), A82 (G), Y86 (F), L135 (I/M). (**C**) Metabolic labeling with [^{3}H]palmitate. AH22*ura3* yeast strain with and without *BET3* plasmids was grown in the presence of [^{3}H]palmitic acid. BET3 and Bet3p were purified and samples were analyzed by SDS–PAGE and fluorography.

these transformants was induced. Loss of Bet3p is lethal and results in only two viable spores if no complementation can be achieved through the transformed constructs. In contrast to human SEDL which complements Trs20p (Gecz *et al*, 2003), BET3 fails to rescue haploid cells with a *bet3* deletion despite the high degree of sequence conservation. Since not only Bet3p but also Bet3p C80S complement a *bet3* knockout (Figure 5C), palmitoylation of Bet3p does not appear to be essential for cell viability. However, the expression of *BET3* under the control of a copper promoter, even when not induced, might lead to a high intracellular level of BET3. A fine-regulatory effect of the palmitoylation on protein stabilization or protein–protein interactions may remain undetected in these cells, when they survive in the absence of a fully functional secretory system.

There is some structural similarity between the palmitate-binding α-helical face of BET3 and the nonspecific lipid-transfer proteins (LTPs) from plants and mammals (Shin *et al*, 1995) although their complete domain folds do not match. The arrangement of three out of the four helices in barley LTP are similar in BET3 (αA, αD and αC in barley LTP are equivalent to α2, α4 and α5 in BET3; Figure 6A) and the bent helix αA in barley LTP is in a position similar to the kinked helix α2 in BET3. In barley LTP, the binding pocket can contract or expand to accommodate lipids or fatty acids of various sizes (Lerche *et al*, 1997; Lerche and Poulsen, 1998). These conformational changes are accompanied by a bending motion in αA and structural adjustments at the C-terminus and helix αC.

In the crystal structure of BET3, the palmitoyl group is completely buried within the α-helical face of the molecule. Based on the structural similarity between BET3 and LTP, we propose a model for the extrusion of the buried palmitoyl group from the hydrophobic pocket. The mechanism, not unlike the structural adjustments described for the LTPs (Lerche *et al*, 1997), involves a rotation of approximately 30° in α2 about a hinge region close to residue G52, coupled with a maximum displacement of approximately 9 Å that would open the pocket and allow the palmitoyl group to slide out of the pocket (Figure 6B). We envisage that this conformational change in α2 will alleviate the extended hydrogen-bonding pattern seen within the putative hinge region of this highly kinked helix and is likely to be triggered by interactions with one or more of the other constituents

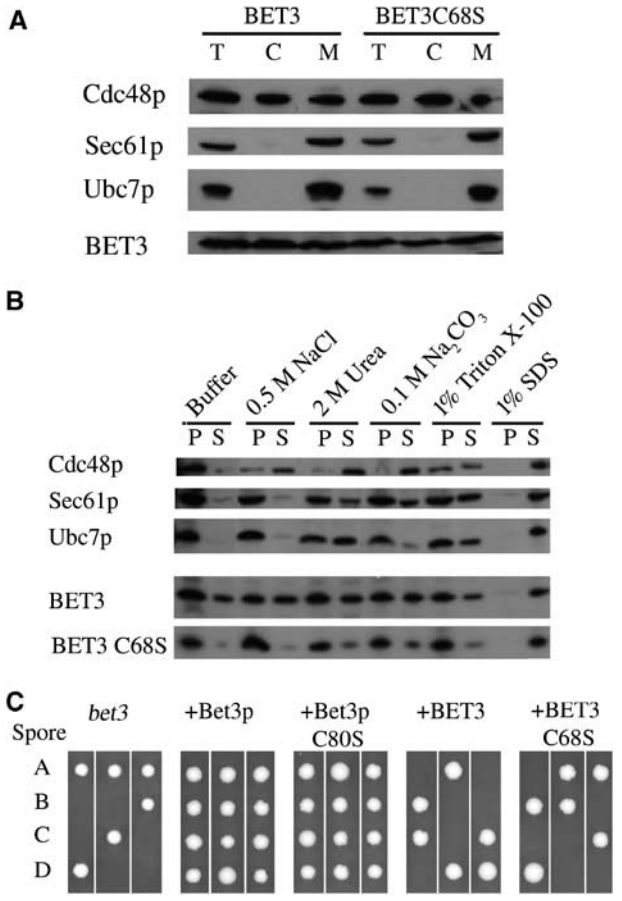

Figure 5 (**A**) Membrane preparations from yeast expressing BET3 and BET3 C68S. Cleared lysates were subjected to ultracentrifugation. Total cell lysate (T), cytosolic (C), and membrane (M, 10-fold concentrated) fractions were analyzed by SDS–PAGE and immunoblotting. (**B**) Membrane extractions of BET3 and BET3 C68S. Membranes were treated with buffer, 0.5 M NaCl, 2 M urea, 0.1 M Na_2CO_3, 1% Triton X-100, or 1% SDS for 30 min on ice. Samples were separated into pellet (P) and supernatant (S) fractions by centrifugation and analyzed by SDS–PAGE and immunoblotting. The integral membrane protein Sec61p and the peripheral membrane-associated proteins Cdc48p and Ubc7p served as reference. (**C**) Tetrad analysis of yeast Y25984 *bet3* deletion strain (EUROSCARF; MAT a/α; *his3Δ1/his3Δ1*; *leu2Δ0/leu2Δ0*; *lys2Δ0/LYS2*; *MET15/met15Δ0*; *ura3Δ0/ura3Δ0*; *YKR068c*::*kanMX4/YKR068c*). Sporulation was induced in cells with and without *BET3* plasmids, and spores were dissected on YPD plates of individual tetrads.

of the TRAPP complex. Interestingly, the two novel motifs, $_{[44]}$LX2#GX2#GX2LXE$_{[57]}$ and $_{[133]}$G#2XGXL$_{[139]}$ (Figure 1; human BET3 numbering), conserved between Bet3p and two other TRAPP components, Trs31p and Trs33p (Sacher *et al*, 2000), are sandwiched together at the interface between α2 and α5 at the exact position of the proposed hinge region. The *bet3-1* mutant that fails to form the TRAPP complex involves alteration of G52 in the first motif, which will perturb the structure of the protein within the proposed hinge region. This suggests an important functional role of the helix kink. The palmitate liberated from the protein in this way would be free to bind to another hydrophobic site such as a membrane bilayer or a binding pocket of another protein. The empty hydrophobic pocket of BET3 could now be available for intermolecular interactions with apolar moieties such as membrane anchors.

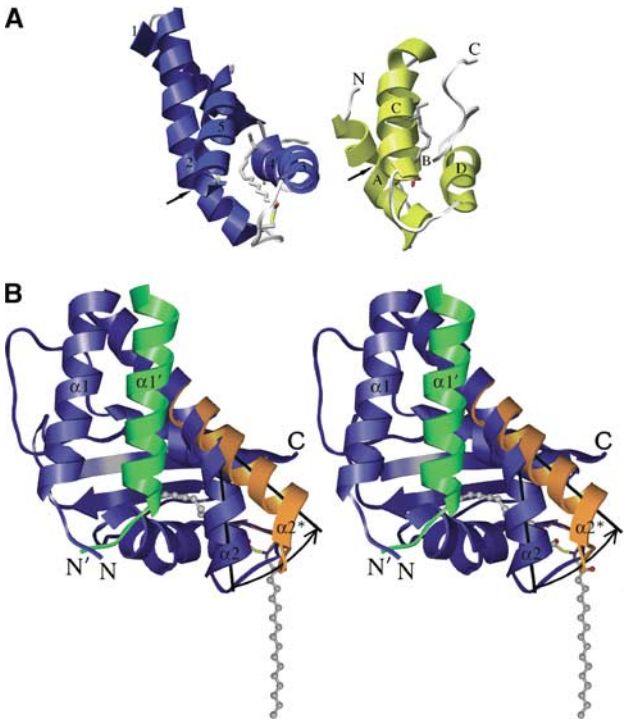

Figure 6 Proposed mechanism for the extrusion of the palmitoyl group from the hydrophobic pocket. (**A**) Structural similarity between the α-helical face of BET3 (blue) and the nonspecific LTP from barley (yellow), here shown with bound palmitate (Lerche and Poulsen, 1998). Helices A, D and C in barley LTP adopt an arrangement similar to helices 2, 4 and 5 in BET3. The arrows point to the kink in helix α2 of BET3 and to a corresponding position within helix αA of the LTP, where a conformational change is observed when the pocket is adjusted for the binding of differently sized lipid-like ligands. (**B**) The BET3 monomer is shown in blue and α1′ from the other subunit of the dimer, that blocks the base of the hydrophobic pocket, is highlighted in green. The palmitoyl group is likely to play a role in membrane association but is, however, completely buried within the α-helical face of the molecule. A rotation of approximately 30° in α2 about a hinge region close to G52, coupled with a maximum displacement of approximately 9 Å, would open the pocket and allow the palmitoyl group to slide out of the pocket. An arrow represents the proposed trajectory of α2, and its new position (α2*) is highlighted in orange. Subsequently, it is envisaged that the pocket will close to exclude the bulk solvent.

Conclusion

The three-dimensional structure of recombinant human BET3, presented here, provides important insights into the molecular basis of TRAPP complex formation and its localization to the *cis*-Golgi membrane. BET3 adopts an α/β-plait topology and a dimeric quaternary organization in solution and is covalently modified with a palmitate moiety attached to residue C68 which is strictly conserved among all BET3 orthologs, suggesting a functional role. We present a model that delineates a mechanism for extraction of the palmitoyl chain from a crevice on the surface of soluble BET3. This will allow subsequent modulation of interaction with the target membrane or binding other molecules. The characterization of Cys-to-Ser mutants of BET3 showed that palmitoylation does not seem to be essential for cell viability and is not required for membrane recruitment of BET3. Since BET3 behaves as a tightly membrane-bound protein, this attachment may be mediated by an additional modification not

present in the crystal structure or through interactions with one of the other components of the TRAPP complex. The hydrophobic cavity of BET3 might also represent a binding pocket for acylated interacting proteins. Finally, a dimeric BET3 defines the stoichiometry of TRAPP, since, for symmetry reasons, it necessitates the recruitment of further dimeric subunits or of pairs of monomeric TRAPP components such as SEDL (Jang *et al*, 2002).

Cloning and expression

The coding sequence of the human *BET3* gene AF041432 (GenBank) was expressed in the yeast *Saccharomyces cerevisiae* under the control of the inducible *CUP*1 promoter of the yeast metallothionein gene. The *BET3* gene was PCR-amplified from the IMAGE clone p998M1228 with gene-specific primers, using the Expand High Fidelity PCR System (Roche, Penzberg, Germany). *Bam*HI and *Not*I restriction sites were introduced into the 5′-end of the forward and reverse primer, respectively. The PCR product was cut at the *Bam*HI/*Not*I site and directionally cloned into the *Bam*HI and *Not*I sites of the yeast expression vector pYEXTHS-BN (Holz *et al*, 2002). The yeast *BET3* gene YKR068c was PCR amplified from AH22*ura3* genomic DNA and cloned accordingly.

Site-directed mutagenesis was performed according to the QuikChange™ mutagenesis protocol essentially as described by Wang and Malcolm (1999). The mutations C68S in BET3 and C80S in Bet3p were introduced using the primers 5′-gctcggtcaaatgttgggaggAgccatgactttcgggaaactgcg-3′ and 5′-gctagaacggcattgccacgcAgtgagaatttagtgaagacaagc-3′, respectively, and reverse complementary oligonucletides. The sequence of mutant clones was verified by DNA sequencing. Standard media and protocol were used for transformation and tetrad analysis (Ausubel *et al*, 1994).

The expression cassette of the resulting plasmid pYEXTHS-BN/BET3 comprised the regulated *CUP*1 promoter, the His_6 tag, the coding sequence of BET3 and the StrepII tag sequence. The plasmid was used to transform *S. cerevisiae* strain AH22*ura3* (MATa, *ura*3Δ, *leu*2-23,112, *his*4-519, *can*1). The resulting transformants were selected on SD-ura medium (2% dextrose, 0.67% yeast nitrogen base (Difco), 40 mg l^{-1} leucine and 40 mg l^{-1} histidine). A yeast transformant harboring the *BET3* expression plasmid (clone 0500000092, internal ID) was grown at 28°C in WMVIII minimal medium supplemented with histidine in a BioFlow3000 3-l fermenter to an optical density (OD_{600}) of 8. Standard fermentation conditions were as described (Prinz *et al*, 2003).

For the production of selenomethionine (SeMet)-labeled protein, the yeast cells were grown in pre-cultures containing 3 mg l^{-1} SeMet. The cultures were grown in BioFlow110 1-l fermenters at 28°C and pH 6.0. 0.5 l WMVIII media containing 50 ml of a 100 × amino-acid solution (Studts and Fox, 1999) and 3 mg l^{-1} SeMet were inoculated as described above and fed-batch fermentation was performed for 19 h. Thereafter, 50 mg l^{-1} SeMet and 1 mM $CuSO_4$ were added to induce gene expression and protein labeling.

Protein purification

The cells were suspended in 40% (w/v) lysis buffer containing 140 mM phosphate buffer, pH 9.0, 300 mM NaCl, 2 mM β-mercaptoethanol and 1 mM PMSF and disrupted by six passages through a high-pressure homogenizer Emulsiflex-05 (Avenstin, Canada) at 6°C and 2000 bar. The cleared lysate (adjusted to pH 7.4) was then subjected to metal-affinity chromatography and StrepTactin-affinity chromatography using an Äkta Explorer (Pharmacia Amersham Biosciences, Germany) at room temperature. BD Talon Super flow matrix (Clonetech, Germany) was used for the metal-affinity chromatography. After application of the protein solution, the column was washed with several volumes of 50 mM phosphate buffer, pH 8.0, 150 mM NaCl, and the protein was eluted with 50 mM phosphate buffer, pH 7.0, 150 mM NaCl, 200 mM imidazol. Absorption at 280 nm, conductivity and pressure were monitored. BET3 was further purified by chromatography using a StrepTactin MacroPrep (IBA, Germany) column after equilibration with 20 mM Tris–HCl, pH 8.0, 150 mM NaCl, 1 mM EDTA. After application, the column was washed with four volumes of the same buffer, and subsequently the protein was eluted using 20 mM Tris–HCl, pH 8.0, 150 mM NaCl, 1 mM EDTA, 2 mM DTT and 2.5 mM D-desthiobiotin (Sigma, Germany). Samples were taken throughout the procedure and analyzed by SDS–PAGE and Western blot.

Metabolic labeling with [^{3}H]palmitate

Strains with BET3 encoding plasmids were grown in WMVIII supplemented with histidine. The AH22*ura3* strain was grown in YPD. Cultures of 25 ml were inoculated at OD_{600} 0.5 and grown to a density of 2.5. To the cells, 500 μCi [^{3}H]palmitate (40–60 Ci mmol^{-1}, Amersham Bioscience, Germany), 1 μg ml^{-1} cerulenin (Sigma) and 1 mM $CuSO_4$ were added and cultures were incubated overnight. Cells were harvested and lysed with glass beads in 50 mM Tris, pH 7.5, 5 mM EDTA, 0.5% SDS and 1 mM PMSF. Lysates were cleared by centrifugation (10 min, 13 000 *g*) and diluted 5-fold with 20 mM Tris, pH 8, 150 mM NaCl, 1 mM PMSF and a pulldown was performed using StrepTactin MacroPrep resin (IBA, Germany) for 1 h at 4°C. Samples were washed with the same buffer and boiled in SDS loading buffer containing 2.5 mM D-desthioboitin. Proteins were separated by SDS–PAGE, the gel was fixated with 10% acetic acid and soaked with Amplify (Pharmacia), dried and subjected to fluorography.

Membrane preparation and extraction

Yeast microsomes were prepared from a crude protein extract obtained by glass bead lysis essentially as described (Panzner *et al*, 1995). For extractions, membranes were treated with 50 mM Tris, pH 7.5, 5 mM EDTA, 1 mM PMSF, or 0.5 M NaCl, 2 M urea, 0.1 M Na_2CO_3, 1% Triton X-100, or 1% SDS and incubated on ice for 30 min. Samples were separated into pellet and supernatant (30 min, 14 000 *g*) and supernatants were subjected to acetone precipitation. Fractions were analyzed by SDS–PAGE and immunoblotting.

BET3 proteins were detected using Penta-His-HRP conjugate (Qiagen). Bands on immunoblots were visualized with enhanced chemiluminescence (ECL, Amersham Bioscience).

Analytical ultracentrifugation and quaternary structure analysis

The molecular mass of BET3 in aqueous buffer was determined using an analytical ultracentrifuge XL-A (Beckman, Palo Alto, CA) equipped with absorbance optics. Samples of approximately 70 μl protein at different concentrations

(0.17–0.62 g l^{-1}) were centrifuged in externally loaded six-channel cells against buffer (15 mM Tris–HCl, pH 8.5, 50 mM NaCl, 0.1 mM EDTA, 0.02% NaN_3, 2 mM DTT) for 2 h at 26 000 r.p.m. (overspeed), followed by 26 h at an equilibrium speed of 22 000 r.p.m. at 10°C. The radial concentration distributions of each sample at sedimentation equilibrium were recorded at three different wavelengths between 275 and 290 nm and fitted globally to equation (1)

$$A_r = A_{rm} e^{MF} \quad (1)$$

with

$$F = \frac{(1-\rho v)\omega^2 (r^2 - r_m^2)}{2RT} \quad (2)$$

using POLYMOLE (Behlke *et al*, 1997). In these equations, ρ is the solvent density, v is the partial specific volume, ω is the angular velocity, R is the gas constant and T the absolute temperature. A_r is the radial absorbance and A_{rm} represents the corresponding value at the meniscus position. When proteins adopt a monomer–dimer equilibrium, the molecular mass M can be treated as a weight average parameter (M_w). In the case of BET3, this value is a composite of the molecular mass values M_m (here 22 584) or M_d and the partial concentrations of monomers, c_m, and dimers, c_d, according to equation (3).

$$M_w = \frac{c_m \cdot M_m + c_d \cdot M_d}{c_m + c_d} \quad (3)$$

from which the equilibrium constant $K_d = c_m^2/c_d$ can be determined.

Crystallization and structure determination

Native BET3 crystals were obtained by the sitting-drop method of vapor diffusion using a 96-well Greiner plate (Crystal Quick™ low profile) at 20°C and drops containing 400 nl of protein (16 mg ml^{-1}) plus 400 nl of reservoir solution equilibrated against 75 µl of reservoir solution. All pipetting steps were carried out using semi-automated dispensing systems (Mueller *et al*, 2001). These crystals grew optimally using 22% PEG 400 as the precipitant in 100 mM Bis–Tris buffer, pH 5.5. Data were collected from a single, flash-frozen native crystal (100 K) to 1.55-Å resolution using a MAR345 imaging plate at the Protein Structure Factory beamline BL-14.2 of Free University of Berlin at BESSY (Berlin, Germany). All data were reduced with DENZO and SCALEPACK (Otwinowski and Minor, 1997). The crystal used for data collection had unit cell parameters $a = 72.9$ Å, $c = 56.8$ Å and belonged to space group $P3_121$ with a monomer in the asymmetric unit. Subsequently, crystals for SeMet-incorporated BET3 (21.9 mg ml^{-1}) were obtained using 25% Jeffamine M600 as the precipitant in 100 mM Na–Hepes buffer, pH 7.0, and peak-wavelength data (0.9797 Å) were collected to 2.5-Å resolution from a single, flash-frozen crystal (100 K). The SeMet crystal was nonisomorphous with respect to the native protein, with unit cell dimensions of $a = 77.0$ Å and $c = 57.7$ Å in $P3_121$. The data collection statistics for the native and SeMet-incorporated BET3 crystals are presented in Table I.

The structure of human BET3 was determined by the SAD approach using the selenium peak wavelength data. Selenium sites were located and initial phases were calculated using SOLVE (Terwilliger and Berendzen, 1999). The phases were subsequently improved by maximum-likelihood density modification implemented in RESOLVE (Terwilliger, 2000). This led to an initial model in which 36 residues were placed and an additional 36 built without side chains (accounting for 72/200 residues). The initial model was extended manually using the program O (Jones *et al*, 1991) and the Se positions as a guide, and led to a model in which 96 residues were placed and an additional 30 built without side chains. After preliminary refinement of the partial SeMet-BET3 structure, the model was placed into the non-isomorphous unit cell of the high-resolution native protein, subsequently refined using REFMAC (Murshudov *et al*, 1997) and then used as a starting model for autotracing of additional amino acids using the program ARP/wARP (Perrakis *et al*, 1999). Several rounds of iterative model building and refinement followed and difference density in the map was assigned as a palmitate molecule conjugated to the protein through a thioester bond to C68. The final model (comprising 159 amino acids, 123 water molecules and a palmitate molecule), refined using data between 30- and 1.55-Å resolution, has an average B-factor of 21 $Å^2$ and an R- and free R-factor of 20.8 and 24.3%, respectively, with good geometry. The refinement statistics are summarized in Table II. The coordinates and diffraction amplitudes have been deposited in the Protein Data Bank with accession code 1SZ7.

Table I X-ray data collection statistics

	SeMet-BET3	BET3
Wavelength (Å)	0.9797	0.9786
Resolution (Å)	30–2.50 (2.59–2.50)	30–1.55 (1.58–1.55)
Total observations	152 879 (44 037)	86 840 (3241)
Unique observations	13 261 (1330)	24 935 (1126)
Completeness (%)	100 (99.8)	97.0 (89.2)
$\langle I/\sigma(I)\rangle$	30.5 (6.4)	20.3 (2.0)
R_{sym}[a]	0.071 (0.508)	0.055 (0.480)

[a]$R_{sym} = \sum_{hkl}\sum_i |I - \langle I_i\rangle| / \sum_{hkl}\sum_i I_i$, where I_i is the intensity of a given measurement and the sums are over all measurements and reflections. Values in parentheses refer to the highest resolution shell.

Table II Refinement statistics

Resolution (Å)	30.0–1.55
R_{work}[a]	0.208
R_{free}[b]	0.243
r.m.s.d. bond distances (Å)	0.012
r.m.s.d bond angles (°)	1.328
Total number of non-H atoms	1230
Av. protein B value ($Å^2$)	21
Number of solvent molecules	123
Av. solvent B value ($Å^2$)	33
Number of ligand atoms	17
Av. ligand B value ($Å^2$)	25

[a]$R_{work} = \sum||F(obs)|-|F(calc)||/\sum|F(obs)|$ for the 95% of the reflection data used in refinement.
[b]$R_{free} = \sum||F(obs)|-|F(calc)||/\sum|F(obs)|$ for the remaining 5%.

Acknowledgements

We thank Patrick Umbach, Anja Koch, Nabila Ibrahim and Ralf Rydschevsky (all from the Protein Structure Factory, Berlin) for their kind help. This work was supported by funding from the German Federal Ministry for Education and Research (BMBF) through the 'Leitprojektverbund Proteinstrukturfabrik' and the Fonds der Chemischen Industrie.

References

Ausubel FM, Brent R, Kingston RE, Moore DD, Seidman JG, Smith JA, Struhl K (1994) *Current Protocols in Molecular Biology*. New York, USA: Greene Publishing Associates and Wiley-Interscience

Barlowe C (1995) COPII: a membrane coat that forms endoplasmic reticulum-derived vesicles. *FEBS Lett* **369:** 93–96

Behlke J, Ristau O, Schönfeld HJ (1997) Nucleotide-dependent complex formation between the *Escherichia coli* chaperonins GroEL and GroES studied under equilibrium conditions. *Biochemistry* **36:** 5149–5156

Bonifacino JS, Glick BS (2004) The mechanisms of vesicle budding and fusion. *Cell* **116:** 153–166

DeLano WL (2003) *The PyMOL Molecular Graphics System*. San Carlos, CA, USA: DeLano Scientific LLC

Dietrich LE, Gurezka R, Veit M, Ungermann C (2004) The SNARE Ykt6 mediates protein palmitoylation during an early stage of homotypic vacuole fusion. *EMBO J* **23:** 45–53

Dunphy JT, Linder ME (1998) Signalling functions of protein palmitoylation. *Biochim Biophys Acta* **1436:** 245–261

Gavin A-C, Bosche M, Krause R, Grandi P, Marzioch M, Bauer A, Schultz J, Rick JM, Michon AM, Cruciat CM, Remor M, Hofert C, Schelder M, Brajenovic M, Ruffner H, Merino A, Klein K, Hudak M, Dickson D, Rudi T, Gnau V, Bauch A, Bastuck S, Huhse B, Leutwein C, Heurtier MA, Copley RR, Edelmann A, Querfurth E, Rybin V, Drewes G, Raida M, Bouwmeester T, Bork P, Seraphin B, Küster B, Neubauer G, Superti-Furga G (2002) Functional organization of the yeast proteome by systematic analysis of protein complexes. *Nature* **415:** 141–147

Gecz J, Shaw MA, Bellon JR, de Barros Lopes M (2003) Human wild-type SEDL protein functionally complements yeast Trs20p but some naturally occurring SEDL mutants do not. *Gene* **320:** 137–344

Gibrat JF, Madej T, Bryant SH (1996) Surprising similarities in structure comparison. *Curr Opin Struct Biol* **6:** 377–385

Glöckner G, Eichinger L, Szafranski K, Pachebat JA, Bankier AT, Dear PH, Lehmann R, Baumgart C, Parra G, Abril JF, Guigo R, Kumpf K, Tunggal B, Cox E, Quail MA, Platzer M, Rosenthal A, Noegel AA (2002) Sequence and analysis of chromosome 2 of *Dictyostelium discoideum*. *Nature* **418:** 79–85

Gönczy P, Echeverri C, Oegema K, Coulson A, Jones SJ, Copley RR, Duperon J, Oegema J, Brehm M, Cassin E, Hannak E, Kirkham M, Pichler S, Flohrs K, Goessen A, Leidel S, Alleaume AM, Martin C, Ozlu N, Bork P, Hyman AA (2000) Functional genomic analysis of cell division in *C. elegans* using RNAi of genes on chromosome III. *Nature* **408:** 331–336

Hay JC, Scheller RH (1997) SNAREs and NSF in targeted membrane fusion. *Curr Opin Cell Biol* **9:** 505–512

Higgins DG, Bleasby AJ, Fuchs R (1992) CLUSTAL V: improved software for multiple sequence alignment. *Comput Appl Biosci* **8:** 189–191

Holm L, Sander C (1993) Protein structure comparison by alignment of distance matrices. *J Mol Biol* **233:** 123–138

Holz C, Hesse O, Bolotina N, Stahl U, Lang C (2002) A micro-scale process for high-throughput expression of cDNAs in the yeast *Saccharomyces cerevisiae*. *Protein Expr Purif* **25:** 372–378

Huang CC, Couch GS, Pettersen EF, Ferrin TE (1996) Chimera: an extensible molecular modeling application constructed using standard components. *Pacific Symp Biocomput* **1:** 724

Ito T, Tashiro K, Muta S, Ozawa R, Chiba T, Nishizawa M, Yamamoto K, Kuhara S, Sakaki Y (2000) Toward a protein–protein interaction map of the budding yeast: a comprehensive system to examine two-hybrid interactions in all possible combinations between the yeast proteins. *Proc Natl Acad Sci USA* **97:** 1143–1147

Jahn R, Lang T, Südhof TC (2003) Membrane fusion. *Cell* **112:** 519–533

Jang SB, Kim Y-G, Cho Y-S, Suh P-G, Kim K-H, Oh B-H (2002) Crystal structure of SEDL and its implications for a genetic disease spondyloepiphyseal dysplasia tarda. *J Biol Chem* **277:** 49863–49869

Jones S, Newman C, Liu F, Segev N (2000) The TRAPP complex is a nucleotide exchanger for Ypt1 and Ypt31/32. *Mol Biol Cell* **11:** 4403–4411

Jones TA, Zou JY, Cowan SW, Kjeldgaard M (1991) Improved methods for building protein models in electron density maps and the location of errors in these models. *Acta Crystallogr A* **47:** 110–119

Kim Y-G, Sohn EJ, Seo J, Lee K-J, Lee H-S, Hwang I, Whiteway M, Sacher M, Oh B-H (2005) Crystal structure of bet3 reveals a novel mechanism for Golgi localization of tethering factor TRAPP. *Nature Struct Mol Biol* **12:** 38–45

Klein SL, Strausberg RL, Wagner L, Pontius J, Clifton SW, Richardson P (2002) Genetic and genomic tools for *Xenopus* research: the NIH *Xenopus* initiative. *Dev Dyn* **225:** 384–391

Lee B, Richards FM (1971) The interpretation of protein structures: estimation of static accessibility. *J Mol Biol* **55:** 379–400

Lerche MH, Kragelund BB, Bech LM, Poulsen FM (1997) Barley lipid transfer protein complexed with palmitoyl-CoA: the structure reveals a hydrophobic binding site that can expand to fit both large and small lipid-like ligands. *Structure* **5:** 291–306

Lerche MH, Poulsen FM (1998) Solution structure of barley lipid transfer protein complexed with palmitate. Two different binding modes of palmitate in the homologous maize and barley non-specific lipid transfer proteins. *Protein Sci* **7:** 2490–2498

Lowe M (2000) Tethers and TRAPPs. *Curr Biol* **10:** R407–R409

Madej T, Gibrat JF, Bryant SH (1995) Threading a database of protein cores. *Proteins Struct Funct Genet* **23:** 356–369

Mammalian Gene Collection (MGC) Program Team (2002) Generation and initial analysis of more than 15 000 full-length human and mouse cDNA sequences. *Proc Natl Acad Sci USA* **99:** 16899–16903

Mueller U, Nyarsik L, Horn M, Rauth H, Przewieslik T, Saenger W, Lehrach H, Eickhoff H (2001) Development of a technology for automation and miniaturisation of protein crystallisation. *J Biotechnol* **285:** 7–14

Murshudov GN, Vagin AA, Dodson EJ (1997) Refinement of macromolecular structures by the maximum-likelihood method. *Acta Crystallogr D* **53:** 240–255

Nichols BJ, Pelham HR (1998) SNAREs and membrane fusion in the Golgi apparatus. *Biochim Biophys Acta* **1404:** 9–31

Otwinowski Z, Minor W (1997) Processing of X-ray diffraction data collected in oscillation mode. *Methods Enzymol* **276:** 307–326

Panzner S, Dreier L, Hartmann E, Kostka S, Rapoport TA (1995) Posttranslational protein transport in yeast reconstituted with a purified complex of Sec proteins and Kar2p. *Cell* **81:** 561–570

Peitzsch RM, McLaughlin S (1993) Binding of acylated peptides and fatty acids to phospholipid vesicles: pertinence to myristoylated proteins. *Biochemistry* **32:** 10436–10443

Perrakis A, Morris R, Lamzin VS (1999) Automated protein model building combined with iterative structure refinement. *Nat Struct Biol* **6:** 458–463

Prinz B, Schultchen J, Rydzewski R, Holz C, Boettner M, Stahl U, Lang C (2003) Establishing a versatile fermentation and purification procedure for human proteins expressed in the yeasts *Saccharomyces cerevisiae* and *Pichia pastoris* for structural genomics. *J Struct Funct Genom* **5:** 29–44

Rossi G, Kolstad K, Stone S, Palluault F, Ferro-Novick S (1995) *BET3* encodes a novel hydrophilic protein that acts in conjunction with yeast SNAREs. *Mol Biol Cell* **6:** 1769–1780

Sacher M, Barrowman J, Schieltz D, Yates III JR, Ferro-Novick S (2000) Identification and characterization of five new subunits of TRAPP. *Eur J Cell Biol* **79:** 71–80

Sacher M, Barrowman J, Wang W, Horecka J, Zhang Y, Pypaert M, Ferro-Novick S (2001) TRAPP I implicated in the specificity of tethering in ER-to-Golgi transport. *Mol Cell* **7:** 433–442

Sacher M, Ferro-Novick S (2001) Purification of TRAPP from *Saccharomyces cerevisiae* and identification of its mammalian counterpart. *Methods Enzymol* **329:** 234–241

Sacher M, Jiang Y, Barrowman J, Scarpa A, Burston J, Zhang L, Schieltz D, Yates III JR, Abeliovich H, Ferro-Novick S (1998) TRAPP, a highly conserved novel complex on the *cis*-Golgi that mediates vesicle docking and fusion. *EMBO J* **17:** 2494–2503

Shin DH, Lee JY, Hwang KY, Kim KK, Suh SW (1995) High-resolution crystal structure of the non-specific lipid-transfer protein from maize seedlings. *Structure* **3:** 189–199

Springer S, Spang A, Schekman R (1999) A primer on vesicle budding. *Cell* **97:** 145–148

Studts JM, Fox BG (1999) Application of fed-batch fermentation to the preparation of isotopically labeled or selenomethionyl-labeled proteins. *Protein Expr Purif* **16:** 109–119

TerBush DR, Novick P (1995) Sec6, Sec8, and Sec15 are components of a multisubunit complex which localizes to small bud tips in *Saccharomyces cerevisiae*. *J Cell Biol* **130:** 299–312

Terwilliger TC (2000) Maximum-likelihood density modification. *Acta Crystallogr D* **56:** 965–972

Terwilliger TC, Berendzen J (1999) Automated MAD and MIR structure solution. *Acta Crystallogr D* **55:** 849–861

Wang W, Malcolm BA (1999) Two-stage PCR protocol allowing introduction of multiple mutations, deletions and insertions using QuikChange™ site-directed mutagenesis. *BioTechniques* **26:** 680–682

Wang W, Sacher M, Ferro-Novick S (2000) TRAPP stimulates guanine nucleotide exchange on Ypt1p. *J Cell Biol* **151:** 289–295

Whyte JR, Munro S (2002) Vesicle membrane complexes in membrane traffic. *J Cell Sci* **115:** 2627–2637

Wood V, Gwilliam R, Rajandream MA, Lyne M, Lyne R, Stewart A, Sgouros J, Peat N, Hayles J, Baker S, Basham D, Bowman S, Brooks K, Brown D, Brown S, Chillingworth T, Churcher C, Collins M, Connor R, Cronin A, Davis P, Feltwell T, Fraser A, Gentles S, Goble A, Hamlin N, Harris D, Hidalgo J, Hodgson G, Holroyd S, Hornsby T, Howarth S, Huckle EJ, Hunt S, Jagels K, James K, Jones L, Jones M, Leather S, McDonald S, McLean J, Mooney P, Moule S, Mungall K, Murphy L, Niblett D, Odell C, Oliver K, O'Neil S, Pearson D, Quail MA, Rabbinowitsch E, Rutherford K, Rutter S, Saunders D, Seeger K, Sharp S, Skelton J, Simmonds M, Squares R, Squares S, Stevens K, Taylor K, Taylor RG, Tivey A, Walsh S, Warren T, Whitehead S, Woodward J, Volckaert G, Aert R, Robben J, Grymonprez B, Weltjens I, Vanstreels E, Rieger M, Schäfer M, Müller-Auer S, Gabel C, Fuchs M, Düsterhöft A, Fritz C, Holzer E, Moestl D, Hilbert H, Borzym K, Langer I, Beck A, Lehrach H, Reinhardt R, Pohl TM, Eger P, Zimmermann W, Wedler H, Wambutt R, Purnelle B, Goffeau A, Cadieu E, Dreano S, Gloux S, Lelaure V, Mottier S, Galibert F, Aves SJ, Xiang Z, Hunt C, Moore K, Hurst SM, Lucas M, Rochet M, Gaillardin C, Tallada VA, Garzon A, Thode G, Daga RR, Cruzado L, Jimenez J, Sanchez M, del Rey F, Benito J, Dominguez A, Revuelta JL, Moreno S, Armstrong J, Forsburg SL, Cerutti L, Lowe T, McCombie WR, Paulsen I, Potashkin J, Shpakovski GV, Ussery D, Barrell BG, Nurse P, Cerrutti L (2002) The genome sequence of *Schizosaccharomyces pombe*. *Nature* **415:** 871–880